A simple three-wave Approximate Riemann Solver for the Saint-Venant–Exner equations

Emmanuel Audusse, Christophe Chalons, Philippe Ung

A simple three-wave Approximate Riemann Solver for the Saint-Venant–Exner equations

E. Audusse * C. Chalons † P. Ung ‡

May 22, 2015

Abstract

The Saint-Venant–Exner equations are widely used in the literature and industrial codes to model the bedload sediment transport. In industrial codes, the resolution of this system of equations is mostly approached by a splitting method which allows a weak coupling between the hydraulic and morphodynamic models but may suffer from stability issues. In recent works, many authors proposed alternative finite volume methods based on a strong coupling to cure this problem. This work pursues two objectives : first we propose a numerical scheme to approximate the solution of the coupled model with a Godunov-type method based on a three-wave Approximate Riemann Solver (ARS) and, second, we extend the purpose to exhibit what is the minimal coupling that ensures the stability of the global numerical process when dealing with collocated finite volume schemes.

Key words. shallow-water equations, Exner equation, splitting method, non-splitting method, approximate Riemann solver, finite volume method, positivity preserving, well-balanced scheme.

Introduction.

The Saint-Venant–Exner system is widely used to model bedload sediment transport phenomenon that occurs in large time and space scales in river hydraulics or coastal studies. It takes the form of a system of three equations where the first two ones are nothing but the shallow water equations with topography and friction source terms whereas the last equation is a simple conservation law that refers to the evolution in time of the topography due to the action of the fluid. Eventually the full system writes

$$\begin{cases} \partial_t h + \partial_x hu = 0, & \text{(1a)} \\ \partial_t hu + \partial_x \left(hu^2 + \dfrac{gh^2}{2} \right) = -gh\left(\partial_x b + T_f\right), & \text{(1b)} \\ \left(1-\Phi\right)\partial_t b + \partial_x q_s = 0, & \text{(1c)} \end{cases}$$

*LAGA, UMR CNRS 7539, Université Paris XIII, Sorbonne Paris Cité, F-93430 Villetaneuse, France – INRIA, ANGE Project-Team, Rocquencourt, F-78153 Le Chesnay Cedex, France – CEREMA, ANGE Project-Team, F-60280 Margny-Lès-Compiègne, France – LJLL, UMR CNRS 7958, UPMC Université Paris VI, ANGE Project-Team, F-75005 Paris, France; http://www.math.univ-paris13.fr/∼audusse/index.html, (audusse@math.univ-paris13.fr).

†LMV, UMR CNRS 8100, Université de Versailles-Saint-Quentin-en-Yvelines, F-78035 Versailles Cedex, France; http://chalons.perso.math.cnrs.fr/, (christophe.chalons@uvsq.fr).

‡MAPMO, UMR CNRS 7349, Université d'Orléans, F-45067 Orléans Cedex 2, France – INRIA, ANGE Project-Team, Rocquencourt, F-78153 Le Chesnay Cedex, France – CEREMA, ANGE Project-Team, F-60280 Margny-Lès-Compiègne, France – LJLL, UMR CNRS 7958, UPMC Université Paris VI, ANGE Project-Team, F-75005 Paris, France; (philippe.ung@math.cnrs.fr).

where the unknowns are the water height $h(t,x)$, the flow velocity $u(t,x)$ and the bottom topography $b(t,x)$. The parameters are the gravitational acceleration g and the porosity of the sediment layer Φ that will be set to zero hereafter. We also introduce the fluid discharge $q(t,x) := h(t,x)\,u(t,x)$. The friction term T_f and the sediment flux q_s are fundamental ingredients of the model since they ensure the coupling between the fluid and the solid parts. They are defined by semi-empirical formulae discussed hereafter.

The friction term T_f is usually defined by semi-empirical formulae. One of the most popular is the Manning-Strickler formula

$$T_f = \frac{|q|\,q}{K_s^2\,h^2\,R_h^{4/3}}, \tag{2}$$

with K_s the Strickler coefficient and R_h the hydraulic radius such that

$$R_h = \frac{l\,h}{l + 2\,h},$$

where l is the width of a rectangular channel. As previously mentioned, this term models the answer of the fluid to the presence of the solid part and is therefore a fundamental ingredient of the coupled model. Note that it will still be neglected in some of the numerical tests to compare the results of the presented scheme with those of the existing literature.

The sediment flux formula q_s is also computed by semi-empirical formulae and is in general a function of the fluid quantities (h,u) only. The number of formulae proposed in the literature is huge and the range of applications of any of them is far from being universal, depending on the nature of the fluid flow and the characteristics of the solid bed. One can exhibit two main categories depending on whether a threshold value is used or not for the sediment transport to start. We will use in the numerical applications the Grass [20] formula

$$q_s(t,x) = A_g|u|^{m-1}u \tag{3}$$

and the Meyer-Peter-Müller formula

$$q_s(t,x) = A_m\,(\tau^* - \tau_c^*)^{3/2} \tag{4}$$

where τ^* refers to a non-dimensional friction term that is weighted by the buoyancy of the sediment particles

$$\tau^* = \frac{\rho_w h T_f}{(\rho_s - \rho_w)d}$$

that is known as the Shields parameter, where ρ_w, ρ_s are the density of the water and solid phase respectively and d the mean granular diameter.

As for the classical shallow water model (with fixed topography), some important stability properties have to be satisfied by a numerical method to approximate correctly the solutions of system (1). In particular, the numerical scheme has to ensure the positivity of the water height and the well-balanced property especially characterized here by the preservation of the lake at rest defined by,

$$\begin{cases} \partial_x(h+b) = 0\,, & (5a) \\ u = 0\,. & (5b) \end{cases}$$

Note that, unlike the shallow water model, the Saint-Venant–Exner equations do not admit any associated energy inequality that could be used to ensure another stability criterion. A last important property is to be able to identify the behavior of the numerical scheme when the sediment transport vanishes since we would like to recover a relevant scheme for the classical shallow water model.

In general, the flux formula q_s makes the morphodynamic equation on b strongly coupled with the hydraulic part of the Saint-Venant–Exner model. As a consequence, the model turns out to be strongly non linear and the eigenvalues and eigenvectors of the corresponding flux Jacobian matrix have no closed algebraic form which makes particularly challenging the design of simple (and coupled) numerical approximation.

Most of the industrial codes [1, 2, 3, 4] are based on this model to perform numerical simulations for sediment transport problems. The core of these software suites is the resolution of hydraulic problems. To take into account the sedimentary aspect, they call sediment modules that are able to solve the Exner equation. The two codes can then run with different numerical parameters such as the time step, the space step or the numerical scheme. They only communicate by exchanging particular data at some given time steps. Such a splitting method works well in particular cases but fails when considering fast flow and introduce numerical instabilities [23, 15, 5].

Another approach was popularized in the early 2000s and consists in solving the Saint-Venant equations and updating the bed topography at the same time steps in order to treat the full system. It will be called *non-splitting method* thereafter. Following the pioneering work of Hudson and Sweby [23], which proposes a suitable coupled method has been the source of a lot of studies. Let us cite the principal ones. Extending the approach developed in [23, 22] where the authors deal with the classical Roe method [31], a lot of works are based on the computation of an approximate Jacobian matrix related to the system (1). Among them, some authors choose to extend classical solvers to systems with source terms, see for example [8] where the authors developed a finite volume non homogeneous Riemann solver (called SRNHS) that is an extension of the VF-Roe scheme, or also [33] where an approximation of the eigenvalues associated to the Jacobian matrix permits to introduce a Riemann solver for (1) based on the HLLC solver. Some other works extend the definition of the Jacobian matrix to the whole system by considering the source term as a non conservative product. This can be done with help of the definition of a family of paths in the plane phase, see [13, 12]. It is also possible to directly derive algebraic conditions to obtain a non-conservative well-balanced Roe solver, see [32, 27]. Some numerical methods have been proposed that avoid the computation of exact Jacobian or Roe matrix. In particular, Delis and coauthors proposed in a serie of papers [16, 26] a scheme that is based on the use of a relaxation model for the Saint-Venant–Exner system (1), which extended the idea introduced in [25]. The relaxation approach has also been studied in [5]. This approach appears quite attractive since it relies on linearized problems that preserve stability properties of the original model and can be used for general sediment flux formulae since the linearized Riemann problem is solved for an homogeneous system that does not involve neither the friction term nor the sediment flux formula, both being treated in a separate step. However its resolution may not be so trivial in practice and the related scheme appears to be more diffusive than other choices. Note that most of these works have been extended to two-dimensional versions of system (1), see [24, 14, 8, 27, 11, 7], including comparisons with industrial software in realistic geometries [26].

The issue concerning the choice between splitting and non-splitting methods is of main interest and was discussed a lot in the last decade. In their early work [23], Hudson and Sweby already justified the introduction of the non-splitted method by opposing some variants of these two strategies to approximate the system (1) (called steady and unsteady approaches). The first assumption leads to a decoupled system in which the hydraulic part is solved first (until an equilibrium is reached) and then the bed topography is updated with help of the previous hydraulic variables. The second idea consists in evaluating simultaneously the water flow and the river bed at the same time step by defining a Roe-type solver based on an approximate Jacobian matrix of the whole system. It appears that the steady approach only works well in situation involving weak interaction between the hydraulic and morphodynamic parts. In general, the unsteady approach does not present this limitation and well behaves for all situations. In [22], the authors extended their analysis to the issue of the choice between splitting and non-splitting approaches, including the case where second order accurate Lax-Wendroff scheme is used to improve the accuracy of the solution (with the help of flux-limiters to avoid spurious oscillations introduced by the higher order scheme they considered). They suggest that for weak values of Froude number, it is preferable to use the splitting approach whereas the non-splitting one is more adapted to high values of Froude number. Cordier et al. bring a further contribution to the discussion in [15] and permit to establish a condition for the hyperbolicity of the model which can be lost at least theoretically for some choice of the sediment flux q_s. Under these assumptions, it appears that for some cases, the numerical instabilities initially observed for splitting methods can be avoided in some cases by a strong limitation on the time step but still not vanish in general. In that context, the authors also suggest to solve the full system with a coupled numerical scheme rather than approximating the solution by a splitting method.

In this work we try to address both aspects. First we propose and analyze a positive and well-balanced three-wave approximate Riemann solver (denoted ARS in the following) that is able to approximate the system (1) and to degenerate to the well-balanced and positive solver introduced in [6] when the sediment flux vanishes (classical Saint-Venant equations). The ARS scheme is introduced as a non-splitting method but does not need the computation of a Jacobian matrix of the full system and then can be used for general sediment flux formula. The ARS scheme is then proved to be at the frontier between the splitting and non-splitting strategies previously introduced as it borrows its philosophy both from the splitting approach for the decoupled calculations of the hydraulic and morphodynamic parts and the non-splitting one for the evaluation of the wave velocities related to the system (1). It allows us to discuss in the last part of the paper what is the minimal quantity of coupling that should be added in industrial codes (in an as less as possible intrusive manner) to stabilize the splitting approach. Numerical tests are presented to exhibit the ability of the ARS scheme to deal with different situations and to enforce our conclusions on the splitting approach.

1 Numerical scheme.

1.1 Generalities on Approximate Riemann Solvers

We describe a Godunov-type finite volume scheme for (1) when the friction term is neglected; its treatment will be described in section 1.9,

$$\begin{cases} \partial_t h + \partial_x hu = 0, & (1.1a)\\ \partial_t hu + \partial_x \left(hu^2 + \dfrac{gh^2}{2} \right) = -gh\partial_x b, & (1.1b)\\ \partial_t b + \partial_x q_s = 0, & (1.1c) \end{cases}$$

Let us first introduce some notations. We consider a sequence of points $x_{i+1/2}$ such that

$$x_{i-1/2} < x_{i+1/2}\,, \quad \forall i \in \mathbb{Z}\,,$$

and we define the cells C_i and space steps $\Delta x_i = \Delta x$, such that

$$C_i = \left]x_{i-1/2}, x_{i+1/2}\right[\,, \quad \Delta x = x_{i+1/2} - x_{i-1/2}\,.$$

In addition, we set $x_i = \left(x_{i-1/2} + x_{i+1/2}\right)/2$.

We also introduce a time step $\Delta t > 0$ that allows to define a sequence of intermediate times t^n by

$$t^{n+1} = t^n + \Delta t\,.$$

Hereafter, X_i^n will denote the approximate cell average of X on the cell $C_i \times [t_i, t_{i+1})$ for all $X = h, hu, b$. At each time t^n and interface $x_{i+1/2}$, one thus faces a Riemann problem between two constant states associated with the cells C_i and C_{i+1}.

Starting from a given piecewise constant approximate solution at time t^n, Godunov-type methods propose to advance the solution at time t^{n+1} in two steps:

- first, to build an approximate solution of the Riemann problem at each interface $x_{i+1/2}$,
- second, to obtain the new solution by evaluating the average value of the juxtaposition of these solutions in each cell C_i at time t^{n+1}.

As an approximate Riemann solution associated with initial data

$$(w(0,x),\, b(0,x))^T = \begin{cases} (w_L,\, b_L)^T\,, & x < 0\,, \quad (1.2)\\ (w_R,\, b_R)^T\,, & x > 0\,, \quad (1.3)\end{cases}$$

with two given states $w_L = (h_L,\, h_L u_L)^T$ and $w_R = (h_R,\, h_R u_R)^T$, we will consider here a simple approximate Riemann solver composed by three waves propagating with velocities $\lambda_L < 0$, $\lambda_0 = 0$ and $\lambda_R > 0$ as shown on the fig. 1,

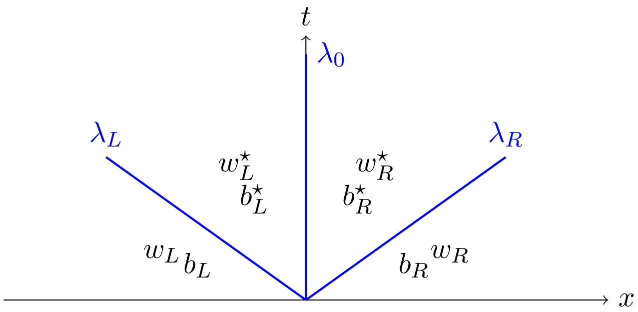

$\lambda_L \leqslant 0 \leqslant \lambda_R$.

Figure 1: Local Riemann solver.

The key point will be the definition of the intermediate states $w_L^\star$, $b_L^\star$, $w_R^\star$, $b_R^\star$. It is known that such an approximate Riemann solver is consistent in the integral sense with (1) [18, 19, 21] provided that the intermediate states satisfy the following consistency relations:

$$f(w_R) - f(w_L) - s\,(w_L,\, w_R,\, b_L,\, b_R) = \lambda_L(w_L^* - w_L) + \lambda_R(w_R - w_R^*)\,, \tag{1.4}$$

with

$$f(w) = (f^h(w),\, f^q(w),\, f^b(w))^T = (hu,\, hu^2 + gh^2/2,\, q_s(w))^T\,, \tag{1.5}$$

and $s(w_L, w_R, b_L, b_R)$ is an approximation of the source term in (1), consistent with $(0,\, -gh\,\Delta b,\, 0)^T$ since it satisfies:

$$\lim_{\substack{w_L,\, w_R \,\to\, w \\ \Delta x \,\to\, 0}} \frac{1}{\Delta x}\, s\,(w_L,\, w_R,\, b_L,\, b_R) = \begin{pmatrix} 0 \\ -gh\partial_x b \\ 0 \end{pmatrix}. \tag{1.6}$$

Then, it is also well-known that the associated Godunov-type scheme is equivalent to the following update formulas, for h^0, u^0, b^0 respectively the water height, the velocity and the bottom topography at the initial state:

$$\begin{cases} (w_i^{n+1},\, b_i^{n+1})^T = (w_i^n,\, b_i^n)^T - \dfrac{\Delta t^n}{\Delta x}(F_{i+1/2}^- - F_{i-1/2}^+)\,, & (1.7)\\ (w_i^0,\, b_i^0)^T = \dfrac{1}{\Delta x}\left(\displaystyle\int_{C_i} h^0(x)dx,\, \int_{C_i}(h^0u^0)(x)dx,\, \int_{C_i} b^0(x)dx\right)^T, & (1.8)\end{cases}$$

with $F^-(w_i,\, w_{i+1},\, b_i,\, b_{i+1})$ and $F^+(w_i,\, w_{i+1},\, b_i,\, b_{i+1})$ the left and right numerical fluxes (see [9]) which will be precised later on, under the well-known CFL condition which ensures that two Riemann problems do not interact

$$\Delta t < \frac{\Delta x}{2\,\max(|\lambda_L|,\, \lambda_R)}\,,$$

where the function max is taken over the set of all considered Riemann problems set at each interface $x_{i+1/2}$.

1.2 Relations defining the intermediate states.

One has to define two intermediate states namely the unknowns $w_L^\star$, $b_L^\star$, $w_R^\star$, $b_R^\star$. We start from the consistency relations (1.4) which write

$$\begin{cases} h_R u_R - h_L u_L = \lambda_L\,(h_L^\star - h_L) + \lambda_R\,(h_R - h_R^\star)\;, & (1.9)\\ \left(h_R u_R^2 + \dfrac{g h_R^2}{2}\right) - \left(h_L u_L^2 + \dfrac{g h_L^2}{2}\right) + g\Delta x\,\{h\partial_x b\} & \\ \qquad\qquad = \lambda_L\,(h_L^\star u_L^\star - h_L u_L) + \lambda_R\,(h_R u_R - h_R^\star u_R^\star)\;, & (1.10)\\ q_s(w_R) - q_s(w_L) = \lambda_L\,(b_L^\star - b_L) + \lambda_R\,(b_R - b_R^\star)\;, & (1.11) \end{cases}$$

where $\{h\partial_x b\}$ stands for a consistent approximation of the source term $h\partial_x b$. Then, we add two continuity relations across the stationary wave which ensure the well-balanced property when no erosion is taken into account, see [6]

$$\begin{cases} h_L^\star + b_L^\star = h_R^\star + b_R^\star\,, & (1.12)\\ h_L^\star u_L^\star = h_R^\star u_R^\star\,. & (1.13) \end{cases}$$

Finally, in order to close the system, we consider a minimization problem for the quantities $b_L^\star$ and $b_R^\star$ in the form

$$\begin{aligned} &\min \mathcal{F}(b_L^\star, b_R^\star) = \left(||b_L - b_L^\star||^2 + ||b_R - b_R^\star||^2\right) \qquad (1.14)\\ &u.c.\ \mathcal{H}(b_L^\star, b_R^\star) = \lambda_L\,(b_L^\star - b_L) + \lambda_R\,(b_R - b_R^\star) - (q_s(w_R) - q_s(w_L)) = 0\,. \end{aligned}$$

In other words, this last relation ensures that the evolution of the bed minimizes a particular moving energy under the consistency constraint (1.11). This modelling of the bottom displacement thanks to an energy minimization problem was also investigated in [10] in a different framework. Eventually, the system of non linear relations (1.9)-(1.10), (1.12)-(1.13) and (1.14) allows us to find the six intermediates states explicitly, see the next subsections. Note that the system can be splitted into two parts since the minimization problem (1.14) can be solved separately and thus defines the values of $b_L^\star$ and $b_R^\star$ that can be used as data in system (1.9)-(1.10), (1.12)-(1.13). We will discuss this property in Section 3.

1.3 Expression of the intermediate states for the solid part

We begin by solving this minimization problem by classically using the Lagrange multipliers. The partial derivatives are given by

$$\frac{\partial \mathcal{F}}{\partial b_L^\star} = -2(b_L - b_L^\star)\,, \qquad \frac{\partial \mathcal{H}}{\partial b_L^\star} = \lambda_L\,,$$

$$\frac{\partial \mathcal{F}}{\partial b_R^\star} = -2(b_R - b_R^\star)\,, \qquad \frac{\partial \mathcal{H}}{\partial b_R^\star} = -\lambda_R\,,$$

$\tilde{\alpha}_1$ is the Lagrange multiplier associated with the single constraint, which gives the following set of equalities

$$\begin{cases} -2(b_L - b_L^*) + \tilde{\alpha}_1 \lambda_L = 0\,, \\ -2(b_R - b_R^*) - \tilde{\alpha}_1 \lambda_R = 0\,, \end{cases} \qquad \Longleftrightarrow \qquad \begin{cases} \tilde{\alpha}_1 = \dfrac{2(b_L - b_L^\star)}{\lambda_L}\,, \\ \tilde{\alpha}_1 = -\dfrac{2(b_R - b_R^\star)}{\lambda_R}\,. \end{cases}$$

Then, one obtains the following equation

$$(b_L - b_L^\star)\lambda_R = (b_R^\star - b_R)\lambda_L, \tag{1.15}$$

which is completed by the constraint $\mathcal{H} = 0$,

$$\Delta q_s = \lambda_L(b_L^\star - b_L) + \lambda_R(b_R - b_R^\star),$$

or equivalently

$$b_L - b_L^\star = \frac{\lambda_R}{\lambda_L}(b_R - b_R^\star) - \frac{1}{\lambda_L}\Delta q_s. \tag{1.16}$$

Solving (1.15)–(1.16) finally defines the values of the bottom topography of the intermediate states as follows,

$$b_L^\star = b_L + \frac{\lambda_L}{\lambda_L^2 + \lambda_R^2}\Delta q_s, \tag{1.17}$$

$$b_R^\star = b_R - \frac{\lambda_R}{\lambda_L^2 + \lambda_R^2}\Delta q_s. \tag{1.18}$$

1.4 Expression of the intermediate states for the hydraulic part

It is now possible to evaluate the remaining unknowns related to the hydraulic part, see [6]. Solving the four equations (1.9)–(1.12)–(1.10)–(1.13), we obtain the values of the water heights,

$$h_L^\star = h_{HLL} + \frac{\lambda_R}{\lambda_R - \lambda_L}\Delta b^\star, \tag{1.19}$$

$$h_R^\star = h_{HLL} + \frac{\lambda_L}{\lambda_R - \lambda_L}\Delta b^\star, \tag{1.20}$$

where h_{HLL} is the intermediate water height of the well-known HLL Riemann solver [21],

$$h_{HLL} = \frac{\lambda_R h_R - \lambda_L h_L}{\lambda_R - \lambda_L} - \frac{1}{\lambda_R - \lambda_L}\left(h_R u_R - h_L u_L\right)\,, \tag{1.21}$$

and the value of the discharge,

$$q^\star := h_L^\star u_L^\star = h_R^\star u_R^\star,$$

$$q^\star = q_{HLL} - \frac{g}{\lambda_R - \lambda_L}\Delta x\{h\partial_x b\}, \tag{1.22}$$

where again, q_{HLL} corresponds to the intermediate discharge of the HLL Riemann solver [21], namely

$$q_{HLL} = \frac{\lambda_R h_R u_R - \lambda_L h_L u_L}{\lambda_R - \lambda_L} - \frac{\left(h_R u_R^2 + \dfrac{g h_R^2}{2}\right) - \left(h_L u_L^2 + \dfrac{g h_L^2}{2}\right)}{\lambda_R - \lambda_L}.$$

1.5 Expression of the numerical fluxes.

Easy calculations using (1.5)–(1.17)–(1.18)–(1.19)–(1.20)–(1.22) give

$$\begin{cases} F^-(w_L, w_R, b_L, b_R) = f(w_L) + \lambda_L\,(w_L^\star - w_L)\ , & \text{(1.23a)} \\ F^+(w_L, w_R, b_L, b_R) = f(w_R) + \lambda_R\,(w_R^\star - w_R)\ . & \text{(1.23b)} \end{cases}$$

At this stage, the scheme is almost entirely defined since only the choice of the extreme wave velocities λ_L and λ_R remains to be specified at each interface $x_{i+1/2}$. Note that when the Grass formula (3) is chosen to define the solid flux q_s, it is well-known [13] that the model is hyperbolic and finding the characteristic speeds of the model consists in calculating the roots of a third degree polynomial equation. However, for numerical purposes, it is sufficient to propose upper bounds of the roots. The computation of these upper bounds is now given. Note that it can be easily extended to the case of more complex sediment flux formulae with a threshold value like (4).

1.6 Approximation of the wave velocities – λ_L and λ_R

Let us recall that for stability reasons, λ_L and λ_R must be upper bounds of the eigenvalues of the Jacobian matrix A of the model; in [33], the authors have proposed some values for the eigenvalues of A, at least approximate ones, for their Riemann solver. Easy calculations give

$$A = \begin{bmatrix} 0 & 1 & 0 \\ gh - u^2 & 2u & gh \\ \tilde{\alpha} & \tilde{\beta} & 0 \end{bmatrix}, \tag{1.24}$$

with $\tilde{\alpha} = \dfrac{\partial q_s}{\partial h}$, $\tilde{\beta} = \dfrac{\partial q_s}{\partial q}$ and $q = hu$.

The exact values of the characteristic speeds are given by the roots of the characteristic polynomial of A, namely

$$p_A(\lambda) = \lambda^3 - 2u\lambda^2 - (gh(1+\tilde{\beta}) - u^2)\lambda - gh\tilde{\alpha} = 0. \tag{1.25}$$

Recall that we are only interested in upper bounds of the exact characteristic speeds, *i.e.* of the solutions of (1.25). Several strategies have been proposed in the literature but most of them are valid under strong assumptions on the polynomial coefficients. Upper bounds proposed by Nickalls [28] turn out to be accurate and can be applied to any polynomial with real roots. It consists in differentiating the polynomial until we obtain a quadratic polynomial, here

$$3\lambda^2 - 4u\lambda - (gh(1+\tilde{\beta}) - u^2) = 0. \tag{1.26}$$

The solutions $\lambda_\pm$ of the corresponding equation can be then divided into two parts x_0 and Ω,

$$\lambda_\pm = x_0 \pm \Omega, \tag{1.27}$$

such as $x_0 = \dfrac{2u}{3}$ and $\Omega = \dfrac{1}{3}\sqrt{u^2 + 3gh(1+\tilde{\beta})}$. In this form, we can exhibit the abscissa of the inflexion point which is equal to x_0, and Ω can be interpreted as the distance in the horizontal direction between the two local extrema of the polynomial (1.25) and the inflexion point. The Nickalls' theorem states that all the roots of (1.25) lie in the range bounded by $x_0 \pm 2\Omega$. That is why, we define the wave velocities by

$$\lambda_L = x_0 - 2\,\Omega, \tag{1.28}$$

$$\lambda_R = x_0 + 2\,\Omega. \tag{1.29}$$

1.7 Positivity of the intermediate water heights.

As far as (1.19) and (1.20) are considered (or used), the positivity of the intermediate water heights is not ensured. We thus propose a similar treatment to the one used in the case of the shallow-water equations [6].

Notice that the signs of $h_L^\star$ and $h_R^\star$ depend on the sign of $\Delta b^\star$. With this in mind, we propose to replace the values of the water heights $h_L^\star$ and $h_R^\star$ by $\tilde{h}_L^\star$ and $\tilde{h}_R^\star$ such that

1. if $\Delta b^\star \geqslant 0$,

$$\lambda_R \tilde{h}_R^\star = \lambda_R \, max\,(h_R^\star, 0)\,, \tag{1.30}$$
$$\lambda_L \tilde{h}_L^\star = \lambda_L h_L^\star - \lambda_R \left(h_R^\star - \tilde{h}_R^\star\right), \tag{1.31}$$

2. if $\Delta b^\star < 0$,

$$\lambda_L \tilde{h}_L^\star = \lambda_L \, max\,(h_L^\star, 0)\,, \tag{1.32}$$
$$\lambda_R \tilde{h}_R^\star = \lambda_R h_R^* - \lambda_L \left(h_L^\star - \tilde{h}_L^\star\right). \tag{1.33}$$

We can easily check that these modifications preserve the positivity of the water heights. Indeed, for the first case, it is clear that $\tilde{h}_R^\star$ is positive. The value of $\tilde{h}_R^\star$ could be $h_R^\star$ or 0. In the first situation, $\tilde{h}_L^\star = h_L^\star$ which is positive, and in the second one,

$$\lambda_L \tilde{h}_L^\star = \lambda_L h_L^\star - \lambda_R h_R^\star \quad \Longleftrightarrow \quad h_R^\star = h_L^\star - \frac{\lambda_R}{\lambda_L} h_R^\star > 0.$$

We apply the same calculations to prove the positivity of the water height in the case $\Delta b^\star < 0$.

1.8 Well-balanced property of the scheme

To ensure this property, we work with the following discretization of the source term already used in [6],

$$\{h\partial_x b\} = \begin{cases} \dfrac{h_L + h_R}{2\Delta x}\, min\,(h_L, \Delta b)\,, & \text{if } \Delta b \geqslant 0\,, \quad (1.34a) \\ \dfrac{h_L + h_R}{2\Delta x}\, max\,(-h_R, \Delta b)\,, & \text{if } \Delta b < 0\,. \quad (1.34b) \end{cases}$$

With this formulation, we can preserve the classical lake at rest.

1.9 Discretization of the friction term

This term is numerically treated in an implicit way for stability purposes [29]. We suppose that q_i^{n+1} is the solution of (1.1) at time t^{n+1}. Then, the solution of (1) $\tilde{q}_i^{n+1}$ at time t^{n+1} is obtained by solving the equation,

$$\tilde{q}_i^{n+1} = q_i^{n+1} - g\,\Delta t \frac{|\tilde{q}_i^{n+1}|\,\tilde{q}_i^{n+1}}{K_s^2\, h_i^{n+1} (R_{h,i}^{n+1})^{4/3}}. \tag{1.35}$$

We suppose that $\tilde{q}_i^{n+1}$ has the same sign as q_i^{n+1} and finally define,

$$\tilde{q}_i^{n+1} = \begin{cases} \dfrac{-1 + \sqrt{1 + 4a\, q_i^{n+1}}}{2a}\,, & \text{if } q_i^{n+1} > 0\,, \quad (1.36) \\ \dfrac{1 - \sqrt{1 - 4a\, q_i^{n+1}}}{2a}\,, & \text{if } q_i^{n+1} \leqslant 0\,, \quad (1.37) \end{cases}$$

with $a = \dfrac{g\,\Delta t}{K_s^2\, h_i^{n+1}\,(R_{h,i}^{n+1})^{4/3}}$.

2 Numerical results.

In order to validate the proposed scheme, called *SimSol* (for "Simple Solver") hereafter, we perform a series of classical test cases from the literature and we extend them to cover additional flow regimes. Thus we study the simulation of dune evolution in fluvial [23, 22, 16, 13, 8, 7], transcritical [15] and torrential [7] flow regimes, and the dam break problem over a moveable bed [27, 5] with or without dry state. For all test cases, we compare our results with those obtained for a scheme based on the computation of an approximate Jacobian matrix and so called Intermediate Field Capturing Riemann solver [30, 17] and an other one based on a relaxation approach [5]. They are respectively referred as to *IFCP* and *Relaxation* thereafter. In addition we consider the widely used Grass formula (3) since it is widely used in the literature. For the last test case we also compare the results with the ones obtained with the two sediment flux formulae (3) and (4).

2.1 Dune evolution in a fluvial flow.

This classical test case is a sediment transport problem which considers a bump under a fluvial flow. The length of the channel is $L = 1000\,m$ and the initial data are parametrized by

$$\begin{cases} b(0,\,x) = \begin{cases} 0.1 + \sin^2\left(\dfrac{(x-300)\pi}{200}\right), & \text{if } 300 \leqslant x \leqslant 500\,m, \\ 0.1\,, & \text{elsewhere}, \end{cases} \\ h(0,\,x) = 10 - b(0,\,x)\,, \\ u(0,\,x) = \dfrac{q_0}{h(0,\,x)}\,, \end{cases}$$

with $q(t,\,0) = q_0 = 10\,m^2/s$ the inflow discharge. Fig. 2 shows the topography at time $T = 700\,s$ with a mesh of 2000 elements. It clearly appears that the proposed scheme is less diffusive compared to the other ones; the relaxation method introduces the highest diffusive effect since no shock front appears and the top of the bump is two times lower than the other values. In addition, the scheme succeeds in computing the shock front. One can also notice that the results returned by this scheme with the wave velocities obtained by the Nickalls' bounds and those approximated by the IFCP solver are quite similar even if the solution associated to the last one is a bit more diffusive.

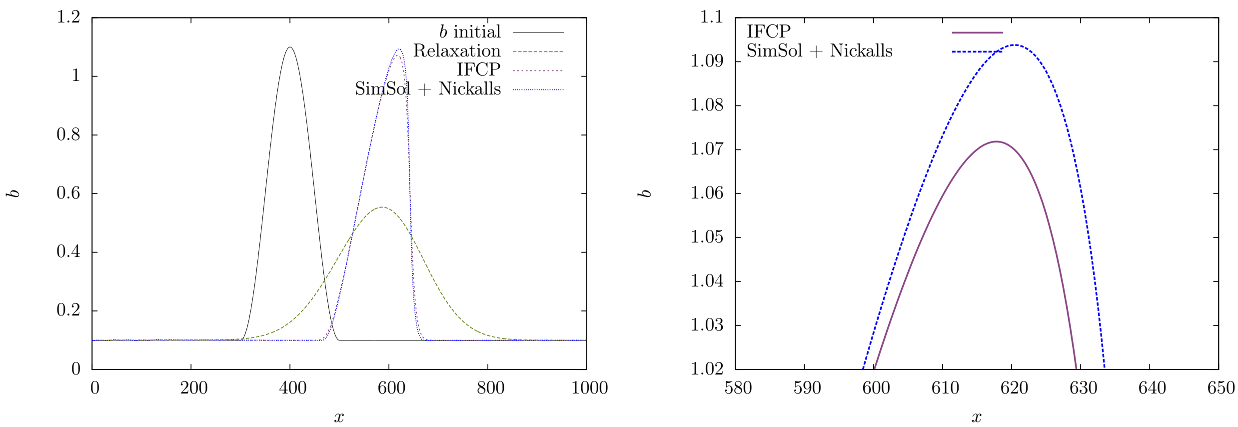

Figure 2: Fluvial flow: Comparison of dune evolution for different numerical schemes.

2.2 Dune (anti-dune) evolution in a torrential flow.

This test case is a modified version of the one presented in [7]. A torrential flow over a moveable bed with an initial bump permits to deal with the anti-dune phenomenon. The channel is $L = 24\,m$ long and the initial bottom topography is

$$b(0,\,x) = \begin{cases} 0.2 - 0.05\,(x-10)^2\,, & \text{if } 8 \leqslant x \leqslant 12\,m, \\ 0\,, & \text{elsewhere.} \end{cases}$$

We impose a uniform discharge $q(0,\,x) = q_0 = 2\,m^2/s$ and evaluate the corresponding water height in the stationary state for the Saint-Venant equations thanks to the Bernouilli's law,

$$\begin{cases} q(t,\,x) = q_0\,, \\ \dfrac{q_0^2}{2\,gh^2} + h + b = H_0 = \dfrac{q_0^2}{2\,gh_0^2} + h_0 + b(0,\,0)\,, \end{cases}$$

with $h(t,\,0) = h_0 = 0.5\,m$. The Grass formula (3) defines the solid flux with parameters $A_g = 0.001$ and $m = 3$. We run the test case with a 2400-element mesh. In this particular test case, the erosion operates after the top of the bump; at this point the velocity is greater than before the top of the dune causing the upstream migration of the anti-dune. The deposition of sediments occurs at the upstream of the bump. Furthermore, the scheme computes well the shock front of the dune and is less diffusive than the relaxation method as shown on fig. 3. In addition, it is noticed that the solutions obtained by the proposed scheme and the IFCP based method share a similar behaviour.

2.3 Dune evolution in a transcritical flow without shock.

This test case describes a transcritical flow without shock over a bump [15]. The length of the channel is $L = 10\,m$ and the initial data are defined by

$$\begin{cases} b(0,\,x) = 0.1 + 0.1\,e^{-(x-5)^2}\,, \\ h(0,\,x) = 0.4 - b(0,\,x)\,, \\ q(0,\,x) = 0.6\,, \end{cases}$$

In fact, we begin by solving the shallow water system by imposing $A_g = 0$ in order to obtain a steady state solution; in our case, we have imposed an intermediate time equal to 20 s. Starting from this last solution, we solve the Saint-Venant–Exner equations by defining the sediment flux q_s using the Grass formula with $A_g = 0.0005$ and $m = 3$. This numerical test gives the results with a 1000-element mesh at time $T = 15$ on fig. 4. We observe an erosion of the dune which mainly operates at the downstream of its top; the lost materials are evacuated at the downstream of the flow. One notes that the relaxation model returns a quite diffusive solution compared to the ones obtained with the proposed solver and the IFCP scheme which both converge to the same solution.

2.4 Dam break over a wet bottom topography.

For this test case, we consider a dam break over a flat wet bottom. We define the Exner law with the Grass formula with parameters $A_g = 0.005$ and $m = 3$. The channel is $10\,m$ long and we impose the following initial conditions,

$$\begin{cases} h(0,\,x) = \begin{cases} 2\,m\,, & \text{if } x \leqslant 5\,m\,, \\ 0.125\,m\,, & \text{if } x > 5\,m\,, \end{cases} \\ u(0,\,x) = 0\,m/s\,, \\ b(0,\,x) = 0\,m\,. \end{cases}$$

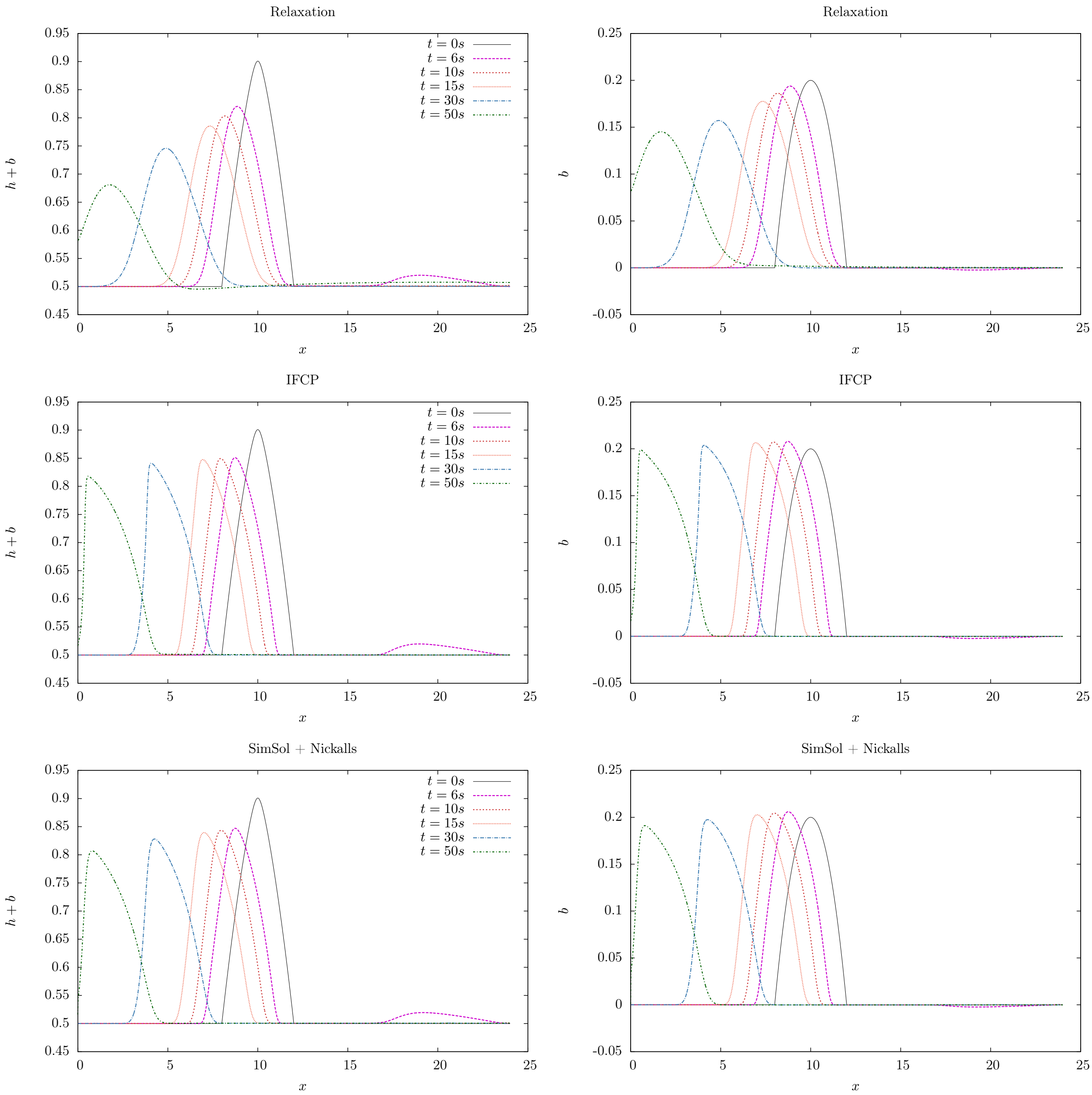

Figure 3: Anti-dune: Comparison of anti-dune evolution for different schemes at different times.

The results on fig. 5 are obtained with a 1000-element mesh at time $T = 1\,s$. This test case has been presented in [5] and has revealed that instabilities appear when we solve the system (1) using a splitting approach; the spurious oscillations result from the fact that the flow reaches a torrential regime in this test case. Here, we do not observe instabilities and the results are similar for the three schemes.

Another interest is the comparison of the results with two different sediment fluxes: the Grass (3) and the Meyer-Peter & Müller (4) formulae. This comparison needs to adapt the Grass' constant to the Meyer-Peter & Müller formula (see [13] for details),

$$A_g = \frac{A_m}{(Rd)^{3/2} K_s^3 \sqrt{h}}, \qquad R = \frac{\rho_s - \rho_w}{\rho_w} \tag{2.1}$$

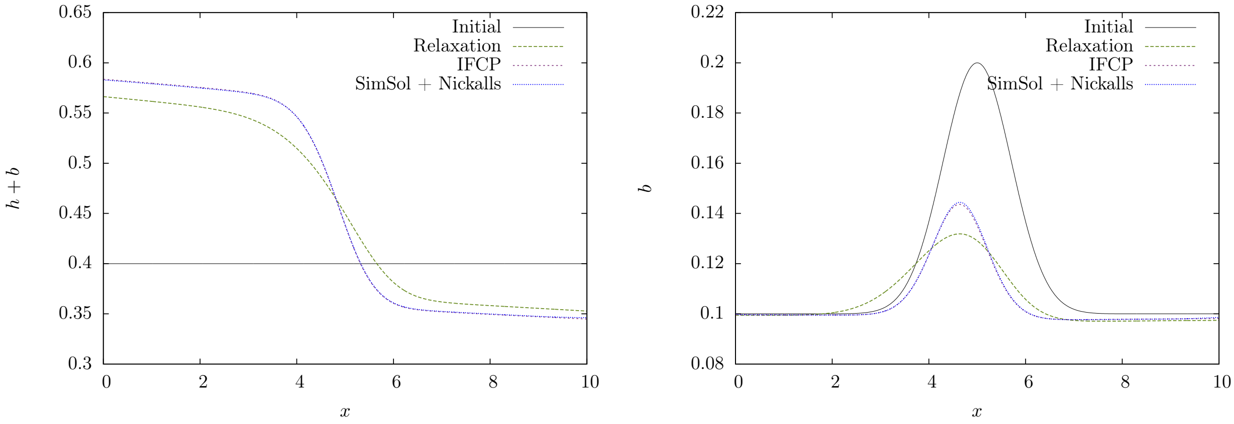

Figure 4: Trancritical flow without shock: Comparison of dune evolution for different numerical schemes.

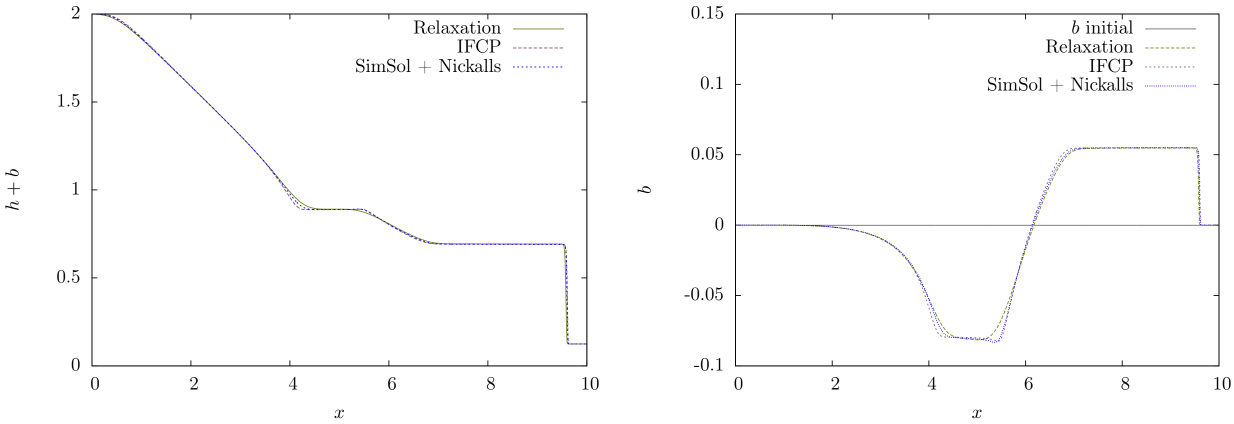

Figure 5: Dam break over a wet bottom: Free surfaces (left) and bottom topographies (right) for different schemes.

where we assume $R_h = h$ (rectangular channel with large width). In fig. 6, it appears that the results are quite similar. We notice that the erosion is a little more pronounced with the Grass formula than the Meyer-Peter & Müller one. It can be explained since the latter considers a threshold value for the Shields parameter under which no sediment is transported. On the contrary, Grass assumes that the bed load transport always occurs.

2.5 Dam break over a dry bottom topography.

The test case is the same as the previous one excepted that the initial water height exhibits dry zone,

$$h(0,\, x) = \begin{cases} 2\,m\,, & \text{if } x \leqslant 5\,m\,, \\ 0\,m\,, & \text{if } x > 5\,m\,. \end{cases}$$

The results in fig. 7 are obtained with a 1000-element mesh at time $T = 1\,s$. For this test case, we consider the friction term in the model (1) to obtain a stable solution (friction term was not included in the previous test cases for the sake of comparisons with results of the literature). Since the relaxation solver and the IFCP one are not adapted to handle vacuum, these schemes are run

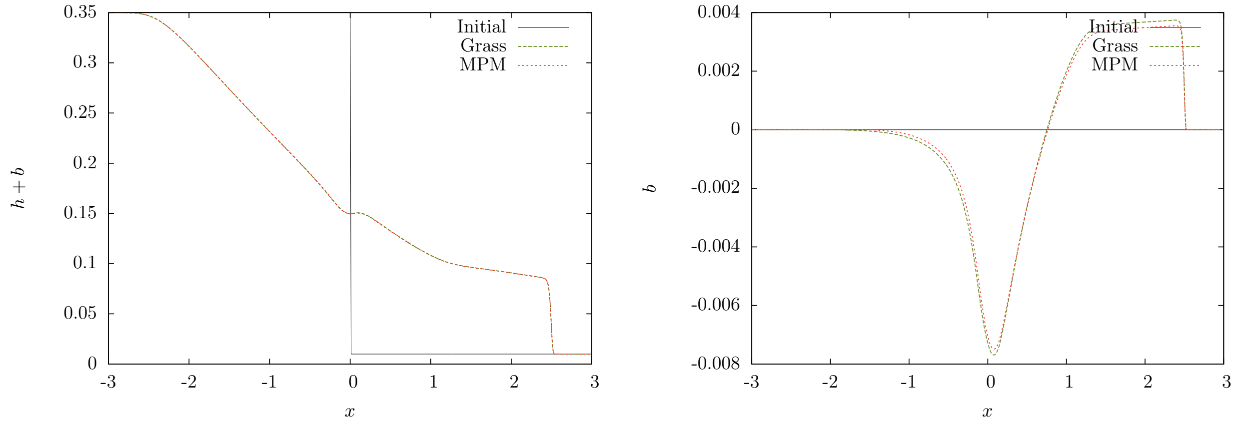

Figure 6: Dam break over a wet bottom: Comparison between the Grass and the Meyer-Peter & Müller formulae for free surfaces (left) and bottom topographies (right).

with a thin layer of water such that,

$$h(0,\,x) = \begin{cases} 2\,m\,, & \text{if } x \leqslant 5\,m\,, \\ 10^{-3}\,m\,, & \text{if } x > 5\,m\,. \end{cases}$$

It is worth underlying that the new ARS scheme works with a classical CFL condition if we impose a low bound for the CFL condition (here, we have set 0.01). Under this condition, we observe that the solution is smooth and does not present instabilities (see fig. 7). In addition, one can notice that the solutions of the proposed scheme and the IFCP solver behave in a similar way whereas the relaxation is a bit more diffusive solution. Within the interval $[4,\,6]$, one observes that erosion strongly occurs at the boundaries of the cavity, which cannot be seen with the relaxation solver.

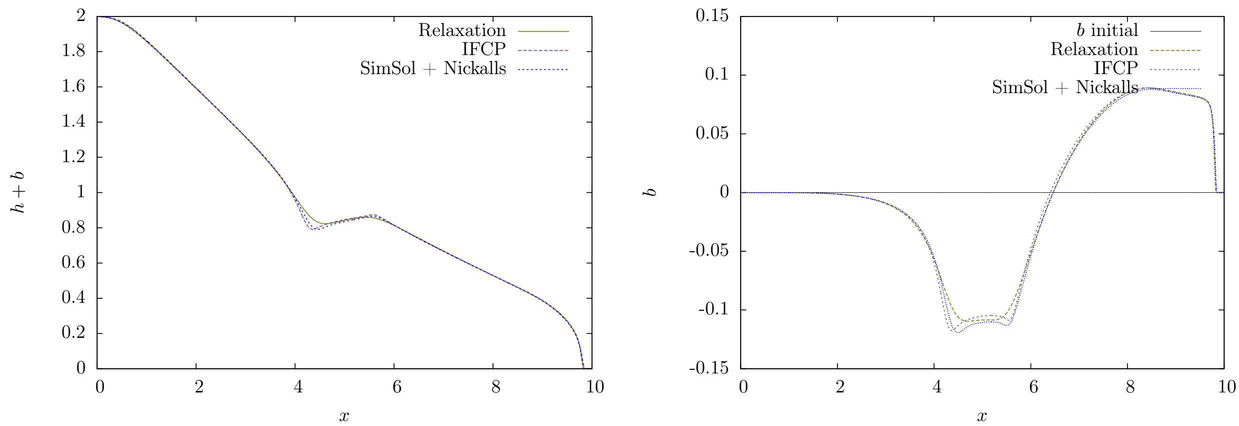

Figure 7: Dam break over a dry bottom: Free surfaces (left) and bottom topographies (right) for different schemes.

3 Numerical strategy : Splitting or not splitting ?

The proposed Godunov-type scheme is at the interface between the splitting and non-splitting methods since we pointed out that

– it is based on a three-wave approximate Riemann solver for the coupled model and the computation of the wave velocities is performed by approximating the eigenvalues of the Jacobian matrix of the whole system (1),
– the computation of the intermediate states is performed in a splitting way by evaluating first the solid quantities through the solution of a constraint energy minimization problem and then the fluid quantities by using the scheme proposed in [6].

Hence it seems legitimate to propose a new contribution to the discussion about the best coupling strategy "splitting or not splitting ?" that was initiated in [23] and pursued in particular in [15], including all the works listed in the introduction and devoted to the derivation of numerical schemes adopting the non-splitting strategy. In all these works, it is emphasized that the splitting strategy is well-adapted for weak and slow interaction between fluid and solid parts but is intrinsically doomed to fail for a large range of test cases. In particular, in [15], the authors exhibit that, unlike the case of the Saint-Venant system, there always exists a negative and a positive eigenvalue for the Saint-Venant–Exner system (1). They conclude that the splitting approach is not able to deal with torrential flows since in this situation, all the eigenvalues of the Saint-Venant systems have the same sign and then the fluid solver relies on a simple upwind strategy. To our opinion, the situation is not so simple since in the splitting strategy, some numerical information is also transported through the discretization of the Exner equation and then one has to consider both fluid and solid discretization strategies. In the following, we investigate numerical strategies where we introduce a slight coupling in a classical splitting approach in order to obtain a stable solver.

The first idea, which is the less intrusive, is to keep unchanged the fluid solver–we already pointed out that it is in general the key idea of industrial software–and to use some outputs to modify the discretization of the Exner equation. More precisely, we propose to adapt the numerical strategy for the Exner equation to the nature of the flow through the computation of the Froude number that characterizes the flow regime. In torrential flow situations, since no information is transported downstream by the flow, one can think of applying a downstream strategy to the discretization of the Exner equation in order to ensure that information is transported in both direction, as it has to be since the coupled system has both positive and negative eigenvalues. As an illustration, we present in fig. 8 the numerical results that are obtained for the three dune evolution test cases of Section 2 when considering a splitting strategy based on
– the ARS scheme [6] for the Saint-Venant system
– an upwind or a downwind strategy for the Exner equation
It appears that in these simple test cases and depending on the proposed discretization of the Exner equation on b, there always exists a stable splitting strategy. Note that one and only one (among the proposed three) strategy is stable and that none of them is stable for the three test cases at the same time. In other words, the coupling between the fluid and the solid parts must take into account the nature of the flow regime. Note that such a coupling might not be easy to extend to (possibly two dimensional) complex flows with flow regimes that may vary in space. The strategy that consists in applying a centered discretization of the Exner equation is shown to be unstable for some test cases hereafter.

Let us now investigate another way to introduce a slight coupling in the splitting strategy by introducing the coupling in the fluid solver and no more in the Exner equation. This second strategy is a direct extension of the proposed scheme in Section 1 and hence works only if an Godunov-type scheme is considered for the fluid part. Let us consider an ARS scheme for the Saint-Venant system–here we will choose the one introduced in [6]–and we simply suggest to modify the computation of the wave velocities that will be no more computed by using an approximation of the eigenvalues of the Jacobian matrix of the Saint-Venant system, but of the eigenvalues of the Jacobian matrix of

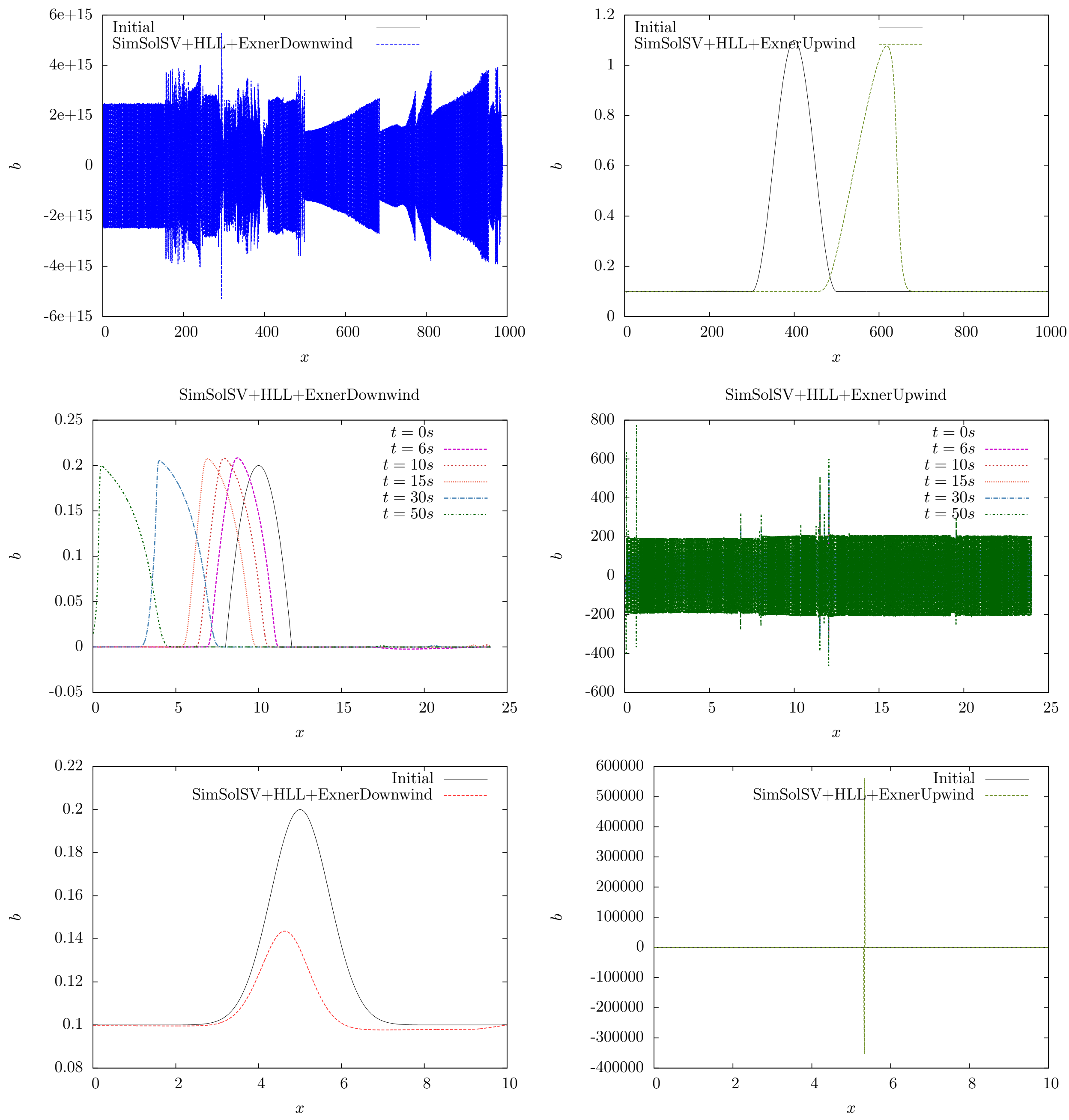

Figure 8: Dune evolution in fluvial (top line), torrential (middle line) and transcritical (bottom line) flow - Comparison of splitting strategy with upwind (left column) or downwind (right column) discretization for Exner equation

the full Saint-Venant–Exner system (1). As an illustration, we compare in the following the results that are obtained for the previous five test cases and with three different numerical strategies,

(i) Use the Godunov-type scheme proposed in [6] with wave velocities λ_L and λ_R based on an approximation of the eigenvalues of the Jacobian matrix of the Saint-Venant system coupled with a centered discretization of the Exner equation. In this case, we use the following values for the computation of the wave velocities

$$\lambda_L = \min\left(u_L - \sqrt{gh_L},\, u_R - \sqrt{gh_R},\, 0\right), \quad \lambda_R = \max\left(u_L + \sqrt{gh_L},\, u_R + \sqrt{gh_R},\, 0\right)$$

(*ii*) Use the Godunov-type scheme proposed in [6] with wave velocities λ_L and λ_R based on an approximation of the eigenvalues of the Jacobian matrix of the full Saint-Venant–Exner system (1) coupled with a centered discretization of the Exner equation. In this case, we compute the wave velocities by using the Nickalls formulae introduced in Section 1.6,

(*iii*) Use the Godunov-type scheme for the full Saint-Venant–Exner system introduced in Section 1.

We designed this comparison to emphasize the difference between the first two approaches (i) and (ii) and thus compare the impact of a slight coupling introduced in the fluid solver. We also compare the results obtained with the new scheme introduced in Section 1 in order to assess two very different discretizations of the solid part. Indeed the fluid strategy is mostly the same in approaches (ii) and (iii) since they both rely on a three-wave ARS and the key point is the way to deal with the Exner equation. In the second approach (ii), the Exner equation is discretized using a classical centered finite difference formula whereas in the third approach (iii), the Exner equation is taken into account through the constraint energy minimization process (1.3).

3.1 Dune evolution in fluvial regime.

Data are given in section 2.1 and every scheme gives a correct solution as shown on fig. 9. Schemes (i) and (ii) are slightly less diffusive. In this flow regime, the coupling between the hydraulic part and morphodynamic part is actually weak and the flow velocity is lower than the extreme characteristic speeds, which explains the efficiency of the splitting method.

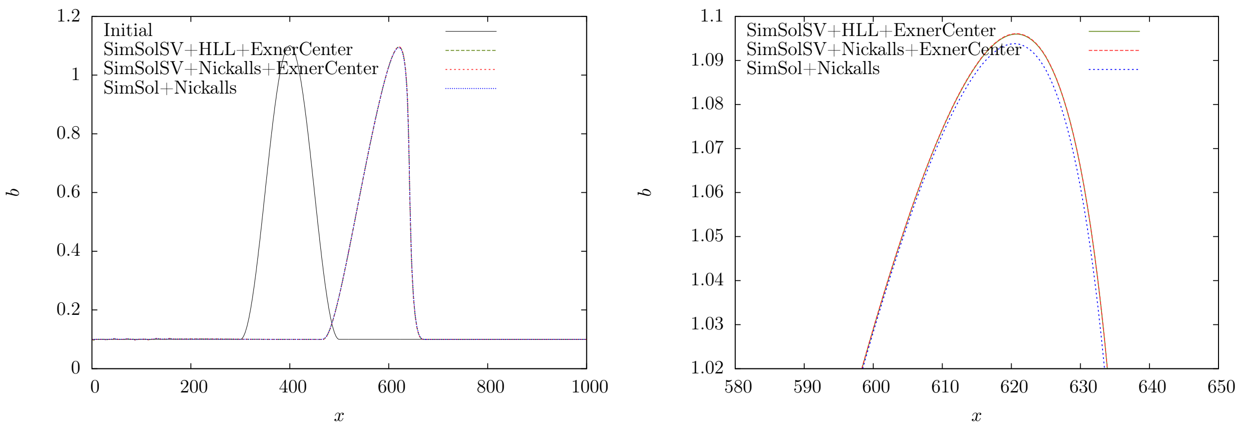

Figure 9: Fluvial flow: Comparison of dune evolution for different numerical schemes.

3.2 Dune (anti-dune) evolution in torrential regime.

Data are given in section 2.2 and lead to a torrential regime. As already pointed out in the literature, in such a flow regime where the flow velocity is higher than the wave velocities, the splitting approach is not efficient. On fig. 10, we observe that the solution is strongly unstable. Nonetheless, the second splitting approach (ii) is stable and gives a solution which is comparable with the one obtained with the new scheme (iii) and to the ones presented on fig. 3 which strongly supports the idea that the splitting method can be efficient, provided that the wave velocities are correctly estimated. Note that modifying the wave velocities does artificially add numerical diffusion since the shock front is preserved.

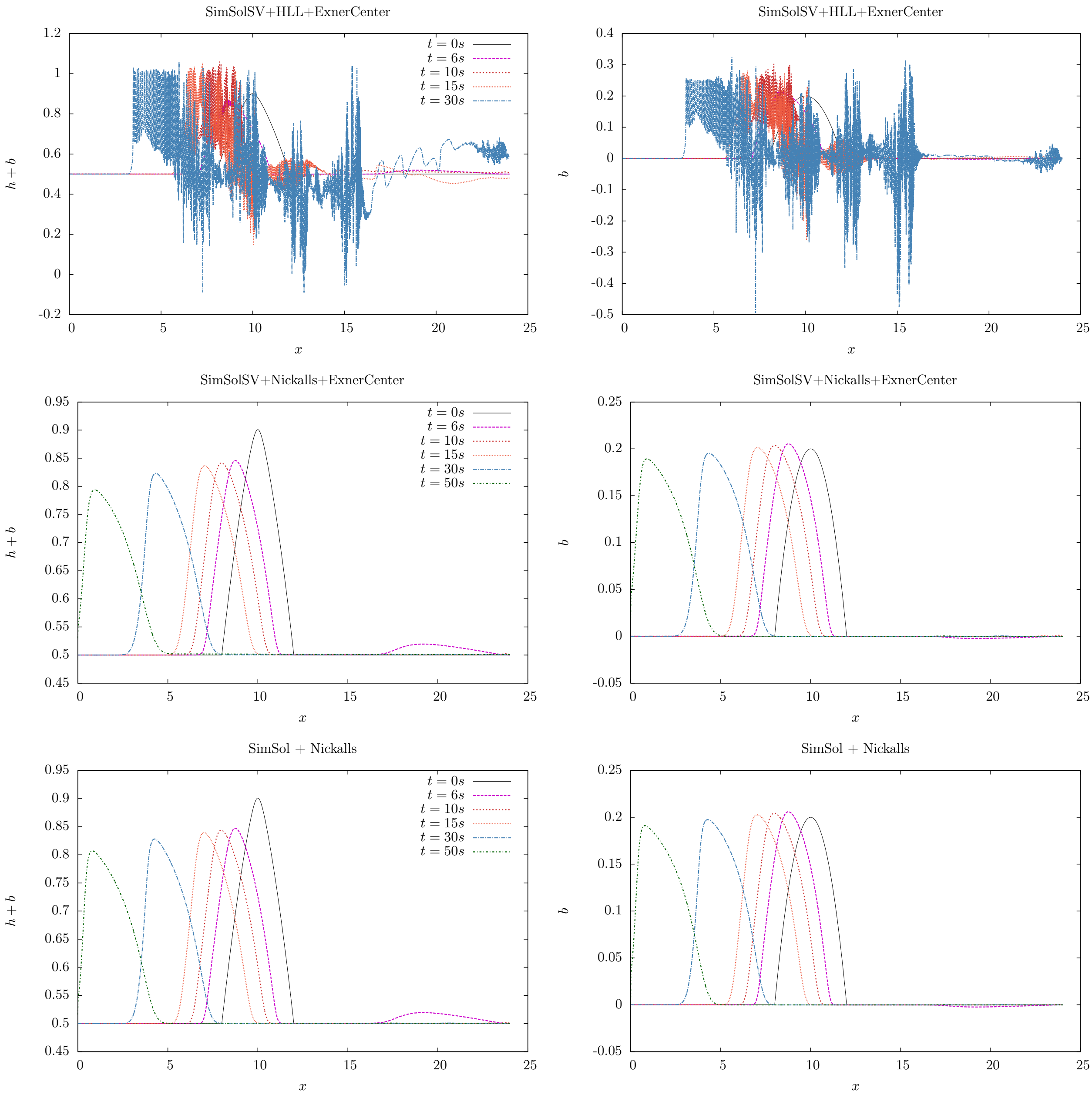

Figure 10: Torrential flow: Comparison of dune evolution for different numerical schemes.

3.3 Dune evolution in transcritical regime without shock.

Data are given in section 2.3. The transcritical regime is pretty interesting since it involves both fluvial and torrential regimes. More precisely, the flow regime changes from fluvial to torrential at the top of the bump since a torrential regime is involved, scheme (i) fails and it is clearly observed on fig. 11 that the unstable zones coincide exactly with the torrential region. Regarding scheme (ii), the results are stable and match those of the new scheme (iii).

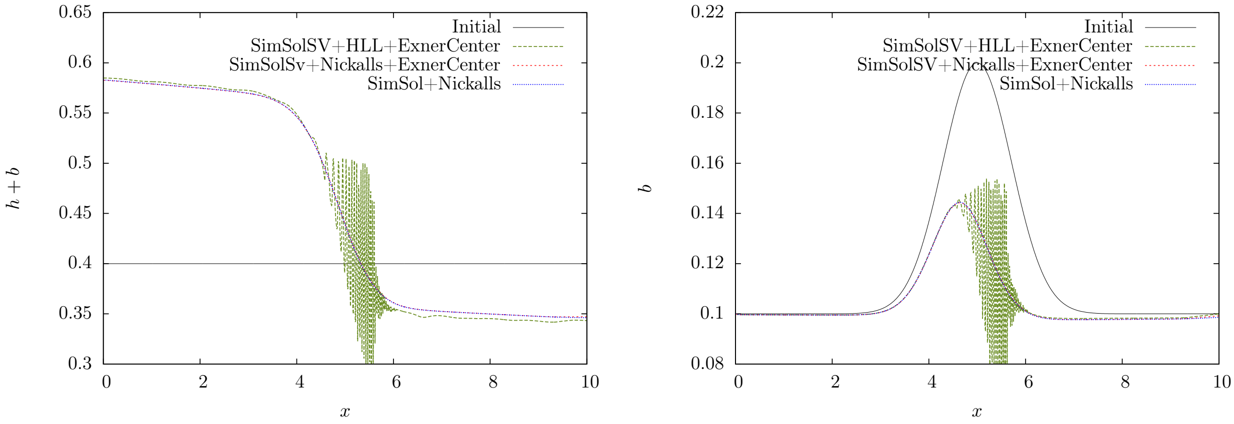

Figure 11: Transcritical flow without shock: Comparison of dune evolution for different numerical schemes.

3.4 Dam break over a wet bottom topography.

Data are given in section 2.4. Scheme (i) fails and produces very pronounced oscillations to the degree that showing the corresponding results would significantly affect the proposed scale on fig. 12. Schemes (ii) and (iii) give similar results in which the shock and the fluvial-torrential transition are properly computed. Again, a proper evaluation of the wave velocities λ_L and λ_R at each interface makes the splitting approach efficient.

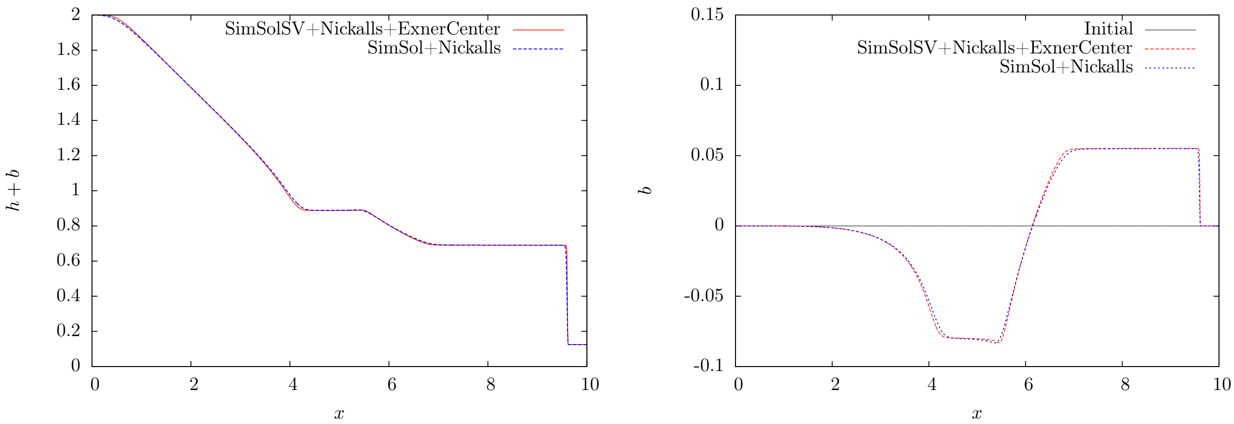

Figure 12: Dam break over a wet bottom: Free surfaces (left) and bottom topographies (right) for different schemes.

3.5 Dam break over a dry bottom topography.

Data are given in section 2.5. As already pointed out, scheme (i) is not efficient for this test case. Again, instabilities appear when the torrential regime is reached, see fig. 13. On the other hand, schemes (ii) and (iii) give similar results which proves again that replacing the wave velocities λ_L and λ_R associated with the Saint-Venant system with those obtained using the Nickalls' upper bounds removes the spurious oscillations of scheme (i) and makes the splitting approach stable and efficient.

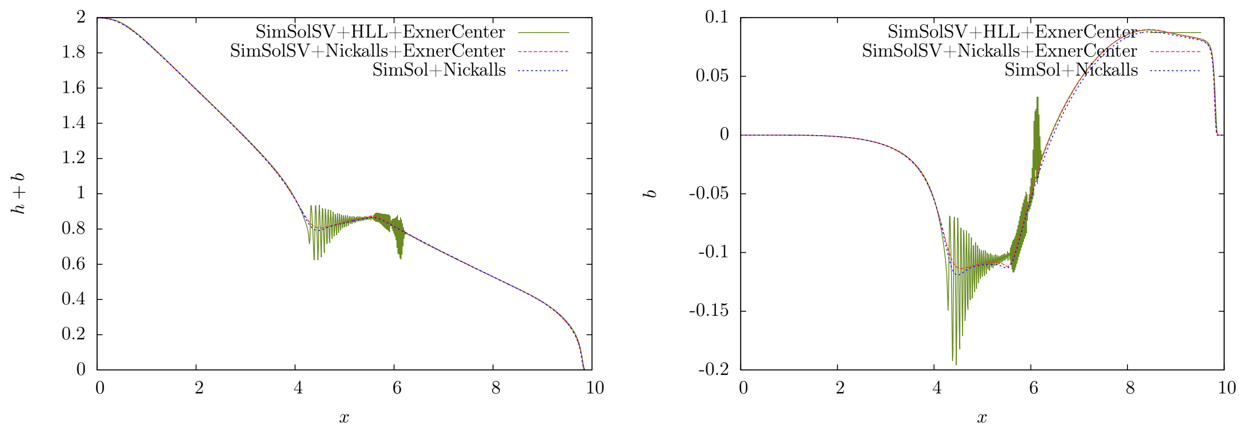

Figure 13: Dam break over a dry bottom: Free surfaces (left) and bottom topographies (right) for different schemes.

4 Conclusion

We have introduced a Godunov-type method based on a new Approximate Riemann Solver for the Saint-Venant–Exner system. The scheme avoids using an approximate Jacobian matrix of the system, has been proved to be positive and well-balanced and has been successfully tested on two families of discriminant numerical test cases.

Moreover this scheme shares common aspects with both splitting and non-splitting approaches that were previously studied in the literature. It helps to go further in the discussion about splitting and non-splitting approaches. In particular we exhibit that a slight modification of the splitting approach, that only consists in changing the wave velocities in the fluid solver, leads to stable simulations for all the test cases we performed. Another modification, that is even simpler since it only modifies the way the Exner equation is dealt with, is shown to ensure stability but not for all test cases.

Acknowledgements. P. U. would like to thank AMIES and EDF for their financial support.

References

[1] Software DELFT3D. http://oss.deltares.nl/web/delft3d.

[2] Software HECRAS. http://www.hec.usace.army.mil/software/hec-ras/.

[3] Software MIKE. http://www.mikebydhi.com/.

[4] Software Telemac-Mascaret. http://www.opentelemac.org/.

[5] E. Audusse, C. Berthon, C. Chalons, O. Delestre, N. Goutal, M. Jodeau, J. Sainte-Marie, J. Giesselmann, and G. Sadaka. Sediment transport modelling: relaxation schemes for Saint-Venant–Exner and three layer models. In EDP Sciences, editor, *ESAIM:Proc.*, pages 80–94, 2012.

[6] E. Audusse, C. Chalons, and P. Ung. A simple well-balanced and positive numerical scheme for the shallow-water system. *Commun. Math. Sci.*, 13(5):1317–1332, 2015.

[7] E. Audusse, O. Delestre, M.H. Le, M. Masson-Fauchier, P. Navaro, and R. Serra. Parallelization of a relaxation scheme modelling the bedload transport of sedi- ments in shallow water flow. In EDP Sciences, editor, *ESAIM: Proc.*, pages 80–94, 2013.

[8] F. Benkhaldoun, S. Sahmim, and M. Seaid. Solution of the sediment transport equations using a finite volume method based on sign matrix. *SIAM J. Sci. Comput.*, 31(4):2866–2889, 2009.

[9] F. Bouchut. *Nonlinear stability of finite volume methods for hyperbolic conservation laws and well-balanced schemes for sources.* Frontiers in Mathematics, 2004.

[10] A. Bouharguane and B. Mohammadi. Minimization principles for the evolution of a soft sea bed interacting with a shallow sea. *Int. J. Comput. Fluid D.*, 26:163–172, 2012.

[11] A. Canestrelli, M. Dumbser, A. Siviglia, and E.F. Toro. Well-balanced high-order centered schemes on unstructured meshes for shallow water equations with fixed and mobile bed. *Adv. Water Resour.*, 33:291–303, 2010.

[12] A. Canestrelli, A. Siviglia, M. Dumbser, and E.F. Toro. Well-balanced high-order centred schemes for non-conservative hyperbolic systems. applications to shallow water equations with fixed and mobile bed. *Adv. Water Resour.*, 32:834–844, 2009.

[13] M. J. Castro-Diaz, E. D. Fernandez-Nieto, and A. M. Ferreiro. Sediment transport models in shallow water equations and numerical approach by high order finite volume methods. *Comput. Fluids*, 37:299–316, 2008.

[14] M. J. Castro-Diaz, E. D. Fernandez-Nieto, A. M. Ferreiro, and C. Pares. Two- dimensional sediment transport models in shallow water equations. a second order finite volume approach on unstructured meshes,. *Comput. Method. Appl. M.*, 198:2520–2538, 2009.

[15] S. Cordier, M. H. Le, and T. Morales de Luna. Bedload transport in shallow water models: Why splitting (may) fail, how hyperbolicity (can) help. *Adv. Water Resour.*, 34:980–989, 2011.

[16] A. I. Delis and I. Papoglou. Relaxation approximation to bed-load sediment transport. *J. Comp. Ap M.*, 213:521–546, 2008.

[17] E. D. Fernández-Nieto, M. J. Castro Díaz, and C. Parés. On an Intermediate Field Capturing Riemann Solver Based on a Parabolic Viscosity Matrix for the Two-Layer Shallow Water System. *J. Sc. Comput.*, 48:117–140, 2011.

[18] G. Gallice. Solveurs simples positifs et entropiques pour les systèmes hyperboliques avec terme source. *C. R. Math. Acad. Sci. Paris*, 334(8):713–716, 2002.

[19] G. Gallice. Positive and entropy stable Godunov-type schemes for gas dynamics and MHD equations in Lagrangian or Eulerian coordinates. *Num. Math.*, 94(4):673–713, 2003.

[20] A. J. Grass. Sediment transport by waves and currents. *SERC London Cent. Mar. Technol.*, (FL29), 1981.

[21] A. Harten, P.-D. Lax, and B. van Leer. On upstream differencing and Godunov-type schemes for hyperbolic conservation laws. *SIAM Review*, 25(1):53–61, 1983.

[22] J. Hudson, J. Damgaard, N. Dodd, T. Chesher, and A. Cooper. Numerical approaches for 1D morphodynamic modelling. *Coast. Eng.*, 52:691–707, 2005.

[23] J. Hudson and P. K. Sweby. Formulations for numerically approximating hyperbolic systems governing sediment transport. *J. Sci. Comput.*, 19:225–252, 2003.

[24] J. Hudson and P. K. Sweby. A high-resolution scheme for the equations governing 2d bed-load sediment transport. *Int. J. Numer. Meth. Fl.*, 47:1085–1091, 2005.

[25] S. Jin and Z. Xin. The relaxation schemes for systems of conservation laws in arbitrary space dimensions. *Commun. Pure Appl. Math.*, 48:235–276, 1995.

[26] G.V. Kozyrakis, A.I Delis, G. Alexandrakis, and N.A. Kampanis. Numerical modeling of sediment transport applied to coastal morphodynamics. *Appl. Numer. Math.*, 2014.

[27] J. Murillo and P. Garcia-Navarro. An exner-based coupled model for two-dimensional transient flow over erodible bed. *J. Comput. Ph.*, 229:8704–8732, 2010.

[28] R. W. D. Nickalls. A new bound for polynomials when all roots are real. *The Mathematical Gazette*, 95(534):520–526, November 2011. www.nickalls.org/dick/papers/maths/bounds2011.pdf.

[29] A. Paquier. *Modélisation et simulation de la propagation de l'onde de rupture de barrage.* PhD thesis, Université Jean Monnet, October 1995.

[30] C. Parés. Numerical methods for nonconservative hyperbolic systems: a theoretical framework. *SIAM J. Numer. Anal.*, 44(1):300–321, 2006.

[31] P.L. Roe. Approximate riemann solvers, parameter vectors and difference schemes. *J. Comput. Phys.*, 43:357–372, 1981.

[32] G. Rosatti, J. Murillo, and L. Fraccarollo. Generalized Roe schemes for 1D two-phase, free-surface flows over a mobile bed. *J. Comput. Ph.*, 227:10058–10077, 2008.

[33] S Soares-Frazao and Y Zech. HLLC scheme with novel wave-speed estimators appropriate for two-dimensional shallow-water flow on erodible bed. *Int. J. Numer. Meth. Fl.*, 66:1019–1036, 2011.